

A Contact SPH Method with High-Order Limiters for Simulation of Inviscid Compressible Flows

Xueying Zhang^{1,*}, Haiyan Tian², Leihsin Kuo² and Wen Chen³

¹ College of Science, Hohai University, Nanjing, Jiangsu 210098, P.R. China.

² Department of Mathematics, University of Southern Mississippi, Hattiesburg, MS 39406, USA.

³ Department of Engineering Mechanics, Hohai University, Nanjing, Jiangsu 210098, P.R. China.

Received 14 December 2011; Accepted (in revised version) 26 September 2012

Communicated by Chi-Wang Shu

Available online 4 January 2013

Abstract. In this paper, we study a class of contact smoothed particle hydrodynamics (SPH) by introducing Riemann solvers and using high-order limiters. In particular, a promising concept of WENO interpolation as limiter is presented in the reconstruction process. The physical values relating interactional particles used as the initial values of the Riemann problem can be reconstructed by the Taylor series expansion. The contact solvers of the Riemann problem at contact points are incorporated in SPH approximations. In order to keep the fluid density at the wall rows to be consistent with that of the inner fluid wall boundaries, several lines of dummy particles are placed outside of the solid walls, which are assigned according to the initial configuration. At last, the method is applied to compressible flows with sharp discontinuities such as the collision of two strong shocks and the interaction of two blast waves and so on. The numerical results indicate that the method is capable of handling sharp discontinuity and efficiently reducing unphysical oscillations.

AMS subject classifications: 76N15, 35L03

Key words: Meshless method, SPH method, the Riemann solution, high-order limiter, Taylor series.

1 Introduction

In the past decade, a number of mesh-free methods such as material point method (MPM) [1], reproducing kernel particle method (RKPM) [2], smoothed particle hydrodynam-

*Corresponding author. *Email addresses:* zhangxy.math@gmail.com (X. Zhang), haiyan.tian@usm.edu (H. Tian), Leihsin.kuo@eagles.usm.edu (L. Kuo), chenwen@hhu.edu.cn (W. Chen)

ics (SPH) [3], radial basis function-based differential quadrature (RBF-DQ) [4], and the method of particular solutions (MPS) [5], have become the most important research topics in computational mechanics. These methods are able to approximate an unknown function or its derivatives on a set of scattered nodes within the local support. Since the meshless methods do not require mesh for spatial discretization, they do not achieve the accuracy of the Riemann-based methods for most ideal gas problems, but they have advantages for many complex problems.

The smoothed particle hydrodynamics (SPH) method is a fully Lagrangian, meshless method which was originally devised to simulate a wide variety of problems in astrophysics involving motion of compressible fluid masses at different spatial scales. Unlike some traditional methods such as finite-difference (FD), finite volume method (FVM) and finite element method (FEM), the SPH is easy to deal with complicated flow phenomena involving arbitrary geometries. Moreover, it is simple for solving two- and three-dimensional problems. The crucial idea of the method is that a smoothing kernel is introduced to approximate functions and their spatial derivatives originating from the interactions of neighboring particles. At present the method has become a useful tool for applications in numerous domains, including free surface and interfacial flows, multi-phase, magnetohydrodynamics, high-velocity impacts, penetration, shock damage in solids and explosion phenomena.

In general, the classical SPH suffers from several perplexing problems, for example, the stability and the consistency issues. The SPH gives shock profiles that are not as sharp as those of exact Riemann solutions and that show unphysical wiggle. In order to achieve high order accuracy, a lot of reformulations of SPH for handling strong shock phenomena were reported. Campbell applied the penalty formulation to enforce the contact condition [6]. Monaghan [7] introduced an artificial viscosity term into the motion and thermal energy equations to handle shocks. Monaghan [8] devised a modified form of the dissipative terms. In this case, the SPH equations were formulated using the total energy equation rather than the thermal energy equation. Inutsuka [9], Parshikov [10, 11], Cha and Whitworth [12] proposed similar schemes where the force acting on each particle is determined by solving the Riemann problem in the vicinity of the midpoint between each pair of interacting particles. This procedure is analog to that employed in Godunov-type schemes which use a Riemann solver to calculate the flux at each cell interface. More recently, Ferrari et al. [13] devised a SPH method that relies on the use of Godunov-type schemes in Lagrangian coordinates. Above methods are the combination of standard SPH with Riemann solutions. Any pair of interacting particles is treated as the left and right states of the Riemann problem, with the changes between the two particles being taken along the line joining them. As expected, the SPH formulations based on Riemann solvers have performed well for solving sharp discontinuities of a variety of shock problems. Sigalotti [14, 15] also provided a family of formulations of SPH which do not rely on Riemann solvers but on an adaptive density kernel estimation (ADKE). The particle distribution is redefined at appropriate intervals in accordance with a previous update of smoothing length. With regard to SPH based on Riemann solvers, any pair of interacting

particles is treated as gradually piece-wise constant where every particle possesses cell which corresponds to the classical piece-wise constant initial condition of the Riemann problem. This means that all of the first and higher-order spatial derivatives of the initial condition for the classical Riemann problem away from the origin vanish identically. So higher-order approximation is necessary for the formations of SPH.

The motivation of the paper is to formulate a family of higher order accuracy SPH, which is stable and efficient for strong and weak shocks as well as rarefaction waves. We intend to reconfigure initial conditions of the Riemann problem by high-order interpolation or alternative fitting method. We introduce three types of limiters based on Taylor series expansions and high-order interpolation. The initial states of the Riemann problem between each pair of interacting particles can be obtained. The contact solvers of the Riemann problem can be achieved by exactly solving Riemann problem, which are used to discrete the fluid dynamic equations. It is obviously different from the classical piece-wise constant data Riemann problem.

2 The outline of classical SPH

2.1 Key formulation

Smoothed particle hydrodynamics is a Lagrangian method which uses the kernel function to approximate physical quantities of each particle in a domain based on the relation of neighbor particles instead of background mesh. A function $f(x)$ is approximated in a continuous form by an integral of the product of the function and a kernel function $W(x-x',h)$ as follows

$$\langle f(x) \rangle = \int_{\Omega} f(x') W(x-x',h) dx'. \quad (2.1)$$

The kernel estimation of the spatial derivative at the point x is

$$\langle \nabla f(x) \rangle = - \int_{\Omega} f(x') \nabla W(x-x',h) dx', \quad (2.2)$$

where $W(x-x',h)$ is a smoothing function that tends to the Dirac delta function as h tends to zero, the brackets " $\langle \rangle$ " denote kernel approximation, h is a parameter that defines the size of the kernel support known as the smoothing length. Using the concept of unitary volume and kernel approximation, we represent the particle approximation for $f(x)$ and its derivative at a point x_i as

$$\langle f(x_i) \rangle = \sum_{j=1}^N \frac{m_j}{\rho_j} f(x_j) W_{ij}, \quad (2.3)$$

$$\langle \nabla f(x_i) \rangle = \sum_{j=1}^N \frac{m_j}{\rho_j} f(x_j) \nabla_i W_{ij}, \quad (2.4)$$

where N is the number of interpolation points within the compact support of radius $3h$, the subscript j refers to a surrounding particle, $W_{ij} = W(x_i - x_j, h)$ and $\nabla_i W_{ij}$ denotes the gradient of $W(x_i - x_j, h)$ with respect to the coordinates of the particle i and $\partial W_{ij} / \partial x_i = \partial W(x_i - x_j, h) / \partial x_i$. The more details of the SPH formation are given in [14, 17, 22]. Since W_{ij} is a function of the distance $r = |x_i - x_j|$ between the particles i and j , we obtain the equation

$$\nabla_i W_{ij} = \frac{\partial W_{ij}}{\partial x_i} = \frac{x_i - x_j}{hr} W'_{ij}, \quad (2.5)$$

where W'_{ij} denotes the first-order derivative with respect to the variable $q = r/h$. According to the relation $\nabla f = \frac{1}{\rho} \nabla(\rho f) - \frac{f}{\rho} \nabla \rho$, an alternative representation of the gradient at particle i is

$$\langle \nabla f(x_i) \rangle = \frac{1}{\rho_i} \sum_{j=1}^N m_j (f_j - f_i) \nabla_i W_{ij}. \quad (2.6)$$

When the above equation is applied to approximate the gradient of pressure in the equation of motion, it is not conservative exactly with regard to momentum. Based on the relation $\nabla f = \rho \nabla(\frac{f}{\rho}) + \rho(\frac{f}{\rho^2}) \nabla \rho$, the symmetrized approximation is obtained,

$$\langle \nabla f(x_i) \rangle = \rho_i \sum_{j=1}^N m_j \left(\frac{f_i}{\rho_i^2} + \frac{f_j}{\rho_j^2} \right) \nabla_i W_{ij}. \quad (2.7)$$

2.2 The discretizations of governing equations

The Euler equations for inviscid gas dynamics in Lagrangian form are given by

$$\begin{cases} \frac{d\rho}{dt} = -\rho \nabla \cdot v, \\ \frac{dv}{dt} = -\frac{1}{\rho} \nabla p, \\ \frac{de}{dt} = -\frac{p}{\rho} \nabla \cdot v, \end{cases} \quad (2.8)$$

where ρ is density, v is the velocity vector, e denotes the specific internal energy and p denotes pressure.

In SPH method, the fluid field is represented as a collection of N particles interacting with each other through evolution equations. Consequently, the equations in Lagrangian framework are respectively discretized by converting the continuous volume integrals to sums over surrounding supporting points in a local domain. The density at particle i is approximated by selecting density summation of neighboring particles according to Eq. (2.3)

$$\rho_i = \sum_{j=1}^N m_j W_{ij}, \quad (2.9)$$

where the summation includes the contribution of particle i itself. Eq. (2.9) is used to discretize the continuity equation. If this form is chosen to calculate the density, variational consistency will demand a symmetrized SPH representation for the equations of motion and thermal energy [12].

The divergence of the velocity $\nabla \cdot v$ is calculated by replacing Eq. (2.4), thus the continuity equation has another approximation of particle as follows

$$\frac{d\rho_i}{dt} = -\rho_i \sum_{j=1}^N \frac{m_j}{\rho_j} v_j^\beta \cdot \frac{\partial W_{ij}}{\partial x_i^\beta}. \quad (2.10)$$

The gradient of 1 being 0 from Eq. (2.3), we have the following approximation of particles

$$\rho_i \sum_{j=1}^N \frac{m_j}{\rho_j} v_i^\beta \cdot \frac{\partial W_{ij}}{\partial x_i^\beta} = 0. \quad (2.11)$$

Obviously, adding the left-hand side of Eq. (2.11) and the right-hand side of Eq. (2.10), we obtain the alternative representation for the continuity equation,

$$\frac{d\rho_i}{dt} = \sum_{j=1}^N \frac{m_j \rho_i}{\rho_j} (v_i^\beta - v_j^\beta) \cdot \frac{\partial W_{ij}}{\partial x_i^\beta}, \quad (2.12)$$

where v_j^β is the β th component of the velocity of the j th interacting fluid particle and x_i^β is the β th Cartesian component of the position vector of the j th interacting fluid particle. Similarly, the discretization of the equation of momentum corresponding to Euler equation without artificial viscosity term and artificial heat conduction term for isentropic flows is

$$\frac{dv_i^\beta}{dt} = \sum_{j=1}^N m_j \frac{p_i - p_j}{\rho_i \rho_j} \frac{\partial W_{ij}}{\partial x_i^\beta}, \quad (2.13)$$

which can be written another form in the following

$$\frac{dv_i^\beta}{dt} = - \sum_{j=1}^N m_j \frac{p_i + p_j}{\rho_i \rho_j} \frac{\partial W_{ij}}{\partial x_i^\beta}. \quad (2.14)$$

The discretization of thermal energy equation can be written as

$$\frac{de_i}{dt} = \sum_{j=1}^N \frac{m_j}{\rho_i \rho_j} p_i (v_i^\beta - v_j^\beta) \cdot \frac{\partial W_{ij}}{\partial x_i^\beta}. \quad (2.15)$$

The thermal energy equation may also be discretized as

$$\frac{de_i}{dt} = \frac{1}{2} \sum_{j=1}^N \frac{m_j}{\rho_i \rho_j} (p_i + p_j) (v_i^\beta - v_j^\beta) \cdot \frac{\partial W_{ij}}{\partial x_i^\beta}. \quad (2.16)$$

In order to ensure variational consistency of the whole scheme, the symmetrized representation for the smoothed version of the thermal energy equation is given as follows

$$\frac{de_i}{dt} = \frac{1}{2} \sum_{j=1}^N m_j \left(\frac{p_i}{\rho_i^2} + \frac{p_j}{\rho_j^2} \right) (v_i^\beta - v_j^\beta) \cdot \frac{\partial W_{ij}}{\partial x_i^\beta}. \quad (2.17)$$

In addition to the above SPH equations, the particle positions are evolved by solving the equation

$$\frac{dx_i^\alpha}{dt} = v_i^\alpha. \quad (2.18)$$

In calculations of compressible fluid, an artificial viscosity term Π_{ij} is added into the discrete equations. This is to dissipate postshock oscillations and to avoid particle interpenetration in high Mach number collisions. An excellent expression has been proposed in [18]. But it may produce errors in the form of excessive heating, which are commonly referred to as '*wall-heating*' errors. In order to reduce excessive wall-heating errors, an artificial heat conduction term H_{ij} is added into the specific internal energy in the literatures [14, 15].

3 Formulations of the method

3.1 The SPH discrete form including contact solution

We want to use the result of the Riemann problem in the vicinity of the position of the contact point A_{ij} relevant to the interactional i th and j th particles in the support domain of i th particle. Researchers such as Parshikov, Cha, Inutsuka and Ferrari have proposed valuable research results [9–13]. This is achieved by modifying the values of v and p . The most effective and direct means to combine SPH and the Riemann problem is to replace p_{ij}^{*n} with p_i and p_j , replace v_{ij}^{*n} with v_i and v_j . The physical variables such as pressure and density of particle i is determined by the physical variables surrounding it. The expressions in Eqs. (2.13) and (2.14) have different forms, so is Eqs. (2.15) and (2.16). Taking into consideration its own contributions to approximation, we assign corresponding weight coefficients positive numbers that are less than 1. So, the SPH equation (2.12)-(2.16) can be converted into discrete forms including contact solution by $p_i + p_j = 2p_{ij}^{*n}$ and $v_i^R + v_j^R = 2v_{ij}^{*n}$,

$$\frac{d\rho_i}{dt} = 2\rho_i \sum_{j=1}^N \frac{m_j}{\rho_j h} (v_{ij}^{*n} - v_i^R) W'_{ij}, \quad (3.1)$$

$$\frac{dv_i^\beta}{dt} = -2 \sum_{j=1}^N \frac{m_j}{\rho_i \rho_j} (p_{ij}^{*n} - \lambda p_i) \frac{\partial W_{ij}}{\partial x_i^\beta}, \quad (3.2)$$

$$\frac{de_i}{dt} = 2 \sum_{j=1}^N \frac{(\mu_1 p_{ij}^{*n} + \mu_2 p_i) m_j}{\rho_i \rho_j h} (v_{ij}^{*n} - v_i^R) W'_{ij}, \quad (3.3)$$

where λ, μ_1 and μ_2 are positive weights that satisfy $0 \leq \lambda \leq 1, \mu_1 + \mu_2 = 1, \mu_i \geq 0$. As a matter of fact, Eq. (3.2) would take a convex combination of (2.13) and (2.14). Also, Eq. (3.3) would take a convex combination of (2.15) and (2.16). It is noted that when choosing $\lambda = 1$ and $\mu_1 = 0$, the contribution to the discretization is entirely derived from (2.13), (2.15) and the contact discontinuity of the Riemann problem. However, an optimal choice of weighted coefficients depends on the specific situation. Supposing, in this method, that the functional values at the reference node i and its supporting node j form a local Riemann problem, thus p_{ij}^{*n} and v_{ij}^{*n} can be obtained by exactly solving Riemann problem. It should be noted here that $\frac{\partial W_{ij}}{\partial x_i^{\beta}}$ or W'_{ij} in Eqs. (3.1)-(3.3) denotes the partial derivative with respect to particle i , not to particle j . In the local region with point i as the centre, the location of the center is fixed, so the partial derivative with respect to particle i is essentially independent of its supporting particle j .

The choice of the smoothing function is related to the accuracy, efficiency and stability of the resulting algorithm. The quintic spline is given as [16]

$$W_{ij} = W(r, h) = \omega_0 \begin{cases} (3-q)^5 - 6(2-q)^3 + 15(1-q)^5, & \text{if } 0 \leq q < 1, \\ (3-q)^5 - 6(2-q)^3, & \text{if } 1 \leq q < 2, \\ (3-q)^5, & \text{if } 2 \leq q < 3, \\ 0, & \text{if } q \geq 3, \end{cases} \quad (3.4)$$

where $q = r/h$ and the normalization factor $\omega_0 = 7/(478\pi h^2)$ for two-dimensional problems. Other kernels such as cubic B-Spline kernel [17], the modified Gaussian kernel [18], and Quadratic kernels [19] have been proposed in related literatures.

3.2 The contact algorithm for interactional particles

In general, the conventional SPH method cannot distinguish the influence from upstream or downstream. To overcome this problem, we take into consideration the directions of wave propagations of the underlying hyperbolic system. Otherwise, non-physical oscillations may be generated near steep gradients. It is noted that the scheme shown in (3.1), (3.3) and (3.3) has only first-order accuracy for spatial approximation supposing that the initial values for the Riemann problem between the reference point and its supporting node remain constants. In terms of the capability of capturing shock, how to construct the high-order Riemann solver is a very critical issue in this study.

Supposing that the Riemann problem is expressed as

$$PDE: \partial_t u + \partial_x f(u) = 0, \quad (3.5)$$

$$IC: u(x, t^n) = \begin{cases} u_L(t^n), & \text{if on one side of } A_{ij}, \\ u_R(t^n), & \text{if on the other side of } A_{ij}, \end{cases} \quad (3.6)$$

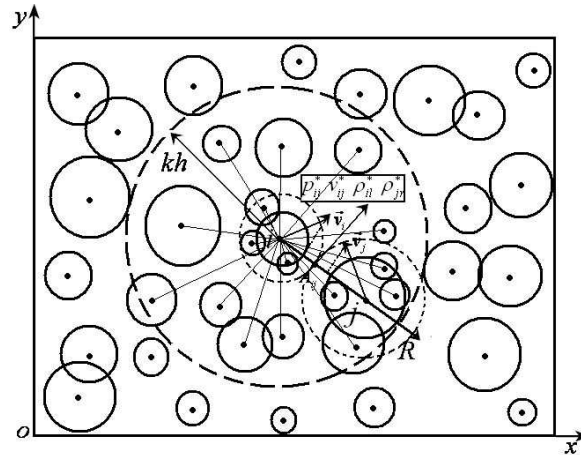


Figure 1: Sketch of interactional particles. Support domain marked with dotted lines for a point x_i is a sphere of a certain radius that relates to the nodal spacing near the point x_i . The contact state at the contact point A_{ij} at the axis R is denoted by $p_{ij}^*, v_{ij}^*, \rho_{ij}^*$ and ρ_{ij}^* . Every interacting particle has its own interpolation stencil surrounding the points i and j .

where initial conditions $u_L(t^n)$ and $u_R(t^n)$ are extrapolated values of the smooth reconstruction functions to both sides of the contact interface A_{ij} , $t = t^n$ denotes current time level.

We introduce a high-order interpolation for the scattered points to reconstruct the initial data of the Riemann problem. In order to further explain this, a local coordinate is designed, whose origin is A_{ij} and whose orientation is along the outer normal from i to j with the axis R . The local interpolation functions $u_i(x)$ and $u_j(x)$ taking particles i and j as their centers can be constructed, respectively. A variation in the value of a physical quantity of each particle i is relevant to every surrounding particle j within the interaction distance kh . As a matter of fact, the particle interaction occurs at the contact interface A_{ij} which is located at the line between the reference particle i and its supporting particle j . The distances from the position of the contact point A_{ij} at the axis R to interactional particles are proportional to their radiuses. Sketch of particle interaction is shown in Fig. 1.

To evaluate the contact states p_{ij}^* and v_{ij}^* in Eqs. (3.1)-(3.3), the data for the Riemann problem first need to be formulated so that correspond to the contact interface A_{ij} between reference point i and its supporting point j . A detailed description of the reconstructed technology will be given in next section.

3.3 The interpolated reconstruction for the Riemann problem

The initial conditions can be reconstructed for the Riemann problem by selecting one-sided stencils from scattered particles. This in particular leads to an improvement upon previous stencil selection strategies [10,11], especially near discontinuities. As a matter of

fact, the quality of the utilized stencils has a significant impact on the performance of the reconstruction. One should consider the following crucial aspects for the selection. First, every stencil should be local relative to its corresponding center i . Second, in smooth regions of the solution the stencils should be isotropic, whereas in non-smooth regions of the solution, one-sided stencils should be preferred in order to avoid interpolation across discontinuities, which would lead to non-physical oscillations. The amount of particles surrounding particle i is uncertain. Moreover, an increasing order of polynomial interpolation gives rise to Runge phenomenon on scattered points.

For simplicity, we first construct a high-order Riemann solver for the one-dimensional compressible flow. Due to randomly distributed knots, it is difficult to employ polynomial interpolation which is usually employed for the mesh-based methods such as finite volume and finite difference. So, we resort to the Taylor series expansion of the function and its derivatives at the reference point or the supporting points to evaluate $u_L(t^n)$ and $u_R(t^n)$.

Take one arbitrary function $f(x)$ as an example, which may be the function of pressure, velocity and other flow variables. The Taylor series expansion with second-order accuracy is given by

$$f(x) = f_s + f'_s \Delta x + \mathcal{O}((\Delta x)^2), \quad x \in (x_{s-\frac{1}{2}}, x_{s+\frac{1}{2}}), \quad (3.7)$$

where the subscript s denotes reference point x_i or supporting point x_j . Let $\Delta s = x_{s+\frac{1}{2}} - x_{s-\frac{1}{2}}$. Unless special treatment is enforced, the spurious numerical oscillation around the discontinuities possibly arises. So, a *limiter* is introduced into the reconstruction process. Accordingly, the function $f(x)$ is then expressed as

$$f(x) = f_s + \frac{\delta f}{\Delta s} \Delta x, \quad (3.8)$$

where $\frac{\delta f}{\Delta s}$ is the approximation of the derivative at the point s with

$$\delta f = \minmod(f_s - f_{s-1}, f_{s+1} - f_s). \quad (3.9)$$

The *minmod* is upwind limiter. We notice that the derivatives in Eq. (3.8) at every knot only have second-order spatial approximation. To achieve higher resolution, δf in Eq. (3.8) is taken as

$$\delta f = \minmod(f_{s+\frac{1}{2}}^- - f_{s-\frac{1}{2}}^-, f_{s+\frac{1}{2}}^+ - f_{s-\frac{1}{2}}^+), \quad (3.10)$$

where $f_{s+\frac{1}{2}}^\pm$ and $f_{s-\frac{1}{2}}^\pm$ denote the left and right values at the interface $x_{s+\frac{1}{2}}$ and $x_{s-\frac{1}{2}}$ of the cell s , which can be reconstructed by WENO5 interpolation which has 5-point stencil and is fifth-order accurate. C. W. Shu gave more details on how to reconstruct such an interpolating function in [20]. The details will not be repeated here.

Another anti-diffusive limiter can be given in the following form

$$\tilde{f}_{s+\frac{1}{2}}^+ = f_s + \minmod(f_{s+\frac{1}{2}}^+ - f_s, f_s - f_{s-1}, f_{s+1} - f_s), \quad (3.11)$$

$$\tilde{f}_{s+\frac{1}{2}}^- = f_{s+1} - \minmod(f_{s+1} - f_{s+\frac{1}{2}}^-, f_{s+1} - f_s, f_{s+2} - f_{s+1}), \quad (3.12)$$

$$\delta f = \minmod(\tilde{f}_{s+\frac{1}{2}}^- - \tilde{f}_{s-\frac{1}{2}}^-, \tilde{f}_{s+\frac{1}{2}}^+ - \tilde{f}_{s-\frac{1}{2}}^+). \quad (3.13)$$

The limiter given by Eq. (3.9) is denoted as *limiter 1*. The limiters in Eqs. (3.10)-(3.13) are denoted as *limiter 2* and *limiter 3*, respectively. In contrast, the anti-diffusive fifth-order WENO reconstruction has an obvious improvement on the smearing of the contact discontinuity and oscillations. With these limiters, the new functional values relating to the reference node i and its supporting node j are reconstructed which form initial data of local Riemann problems. The exact Riemann solver $p_{ij}^*, v_{ij}^*, \rho_{il}^*$ and ρ_{jr}^* can be obtained at the contact point A_{ij} by exactly solving one-dimensional Riemann problem (3.5) and (3.6). Solving process for the Riemann problem will not be repeated again, see [21] for more details.

As for the extension of the method to multidimensional problems, the generalization of the scheme is not straightforward. Due to arbitrary distribution of scattered particles, it is troublesome to reconstruct the initial data of the Riemann problem. We may do this through the RBF interpolation for the scattered points or the Taylor series expansion. In the latter case, take a two-variable function $f(x, y)$ as an example, the Taylor series expansion with second-order accuracy is given by

$$f(x, y) = f(x_s, y_s) + f_x(x_s, y_s)\Delta x + f_y(x_s, y_s)\Delta y + \mathcal{O}(\rho^2), \quad (3.14)$$

where $\rho = \sqrt{\Delta x^2 + \Delta y^2}$, the subscripts s denotes reference point (x_i, y_i) or supporting point (x_j, y_j) . Similarly, the two partial derivatives at the point (x_s, y_s) in Eq. (3.14) can be approximated by introducing upwind limiter. Suppose the derivative $f_x(x_i, y_i)$ can be denoted as

$$f_x(x_i, y_i) = \frac{\delta f}{\Delta x}, \quad (3.15)$$

where $\delta f = \minmod(f_i - f_j)$, $j = 1, 2, \dots, N_i$. As shown in Fig. 1, N_i denotes the number of supporting points within the interaction distance kh .

4 Numerical tests

In the section we present numerical examples as applied to one dimensional compressible Euler equation to validate effectiveness of the proposed SPH method. We provide some examples with strong discontinuities. For comparisons we also run the conventional SPH, the contact SPH (HSPH) algorithm, the contact SPH with three kinds of limiters. All SPH computational schemes do not include artificial viscosity term and artificial heat conduction term. The smooth length is taken as $h_{ij} = (h_i + h_j)/2$.

4.1 The Sod shock-tube problem

At first, we suppose a diaphragm is located at $x=0$ which separates two regions of constant density and pressure. The initial conditions are given by $\rho_L = 1.0, p_L = 1.0, e_L = 2.5$ for left state ($x < 0$) and $\rho_R = 0.25, p_R = 0.1795, e_R = 1.795$ for right state ($x > 0$). The same initial parameters were used in [14]. The gas on the left of the initial discontinuity is represented by 320 particles of equal mass, yielding a uniform spacing $\delta x = 0.001875$ and the remaining 80 particles were placed to the right side yielding a uniform spacing $\delta x = 0.0075$ covering the interval $-0.6 \leq x \leq 0.6$. The compressible fluid satisfies ideal gas equation of state written as $p = (\gamma - 1)\rho e$, where γ is the adiabatic index. Fig. 2 shows the results at $t = 0.25$ when the diaphragm broken flashily.

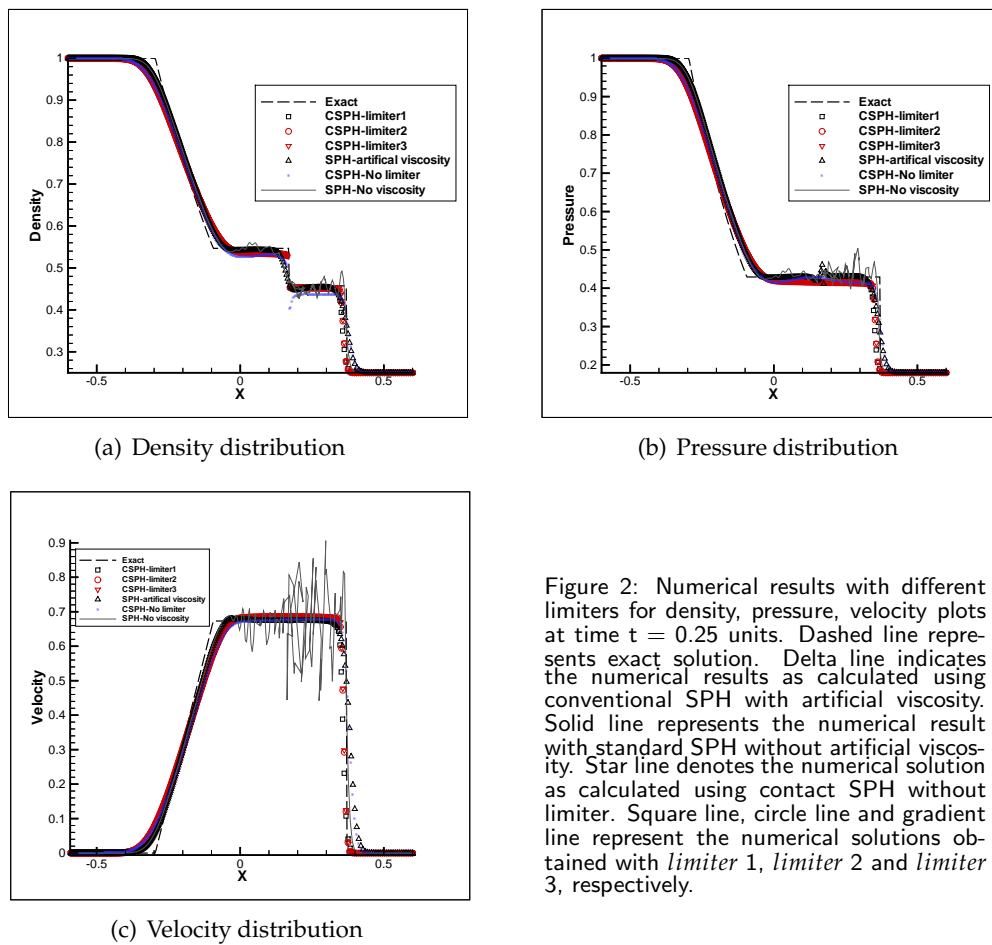


Figure 2: Numerical results with different limiters for density, pressure, velocity plots at time $t = 0.25$ units. Dashed line represents exact solution. Delta line indicates the numerical results as calculated using conventional SPH with artificial viscosity. Solid line represents the numerical result with standard SPH without artificial viscosity. Star line denotes the numerical solution as calculated using contact SPH without limiter. Square line, circle line and gradient line represent the numerical solutions obtained with *limiter 1*, *limiter 2* and *limiter 3*, respectively.

We may see that the initial discontinuity evolves into three types of discontinuities consisting of rarefaction wave, contact discontinuity and shock wave. In particular, when a classical SPH scheme without artificial viscosity is employed, the profiles denoted by

solid lines for density, pressure and velocity are severely affected by the presence of unphysical wiggles near the contact discontinuity and shock wave. Furthermore, the linear stability of the method is clearly affected by the artificial viscosity. The amplitude of the numerical oscillations is reduced when the artificial viscosity is introduced, see the lines denoted by symbol ' Δ '.

It is noted that the excessive numerical diffusion across several points arises from the density plots at both the shock and contact discontinuity. When the contact solutions of Riemann problem and three kinds of limiters are used, we may see that higher accuracy and steeper representation of wave front can be achieved, see the density plot. The lines denoted by symbols ' \square ', ' \circ ' and ' ∇ ' indicate respectively the calculated solutions with '*limiter1*', '*limiter2*' and '*limiter3*', which reproduce the exact ones (dashed lines) with very good accuracy.

4.2 The shock-tube problem

We further test another shock-tube problem by using different numbers of particles and initial conditions of the Riemann problem. It can be seen that the left and the right regions of the tube are separated by a diaphragm which is filled by the same gas with different physical states. After bursting of the diaphragm, the discontinuity breaks into leftward moving and rightward moving waves, which are separated by a contact discontinuity. The initial conditions are given by $\rho_L = 1$, $p_L = 1$, $v_L = 0$ for left-side state $x < 0$ and $\rho_R = 0.125$, $p_R = 0.1$, $e_R = 0$ for right-side state $x > 0$, with $\gamma = 1.4$. Note that the same initial parameters were used in [21]. The 600 uniformly distributed particles are placed on each side of the initial discontinuity. The spatial range is $-0.6 \leq x \leq 0.6$. The initial spatial step is uniformly $\Delta x = 0.002$. The initial smoothing length is set to $h_0 = 3\Delta x$. The calculation was carried out with a constant time step $\Delta t = 2.5 \times 10^{-4}$.

The solution profiles are shown in Fig. 3 for density, velocity and pressure as compared to the exact ones denoted by dashed lines at $t = 0.24$. The proposed contact SPH with limiters can give steep representation of wave fronts that has the ability of capturing the possible discontinuity and shock wave.

4.3 The shock-tube with a strong shock

The test model deals with a Riemann problem whose initial data are given by $\rho_L = 1.5 \times 10^3$, $v_L = 0$, $p_L = 3.0 \times 10^4$, $e_L = 10.0$ for left-side state $x < 0$ and $\rho_R = 1.2 \times 10^3$, $v_R = 0$, $p_R = 1.0 \times 10^4$, $e_R = 4.16667$ for right-side state $x > 0$, with $\gamma = 1.4$, see [11]. The calculation is implemented by using 400 distributed particles. 320 particles are uniformly placed on the left side of $x = 0$ and 80 particles on the other side. The computational interval is $-0.6 \leq x \leq 0.6$. The time step is $\Delta t = 0.0004$. The numerical solutions are shown in Fig. 4 as compared to the exact one denoted by dashed line at $t = 0.04$.

The solution to this problem consists of a left moving shock, moving slowly to the left, a right traveling contact discontinuity and a shock wave moving to the right. We see that

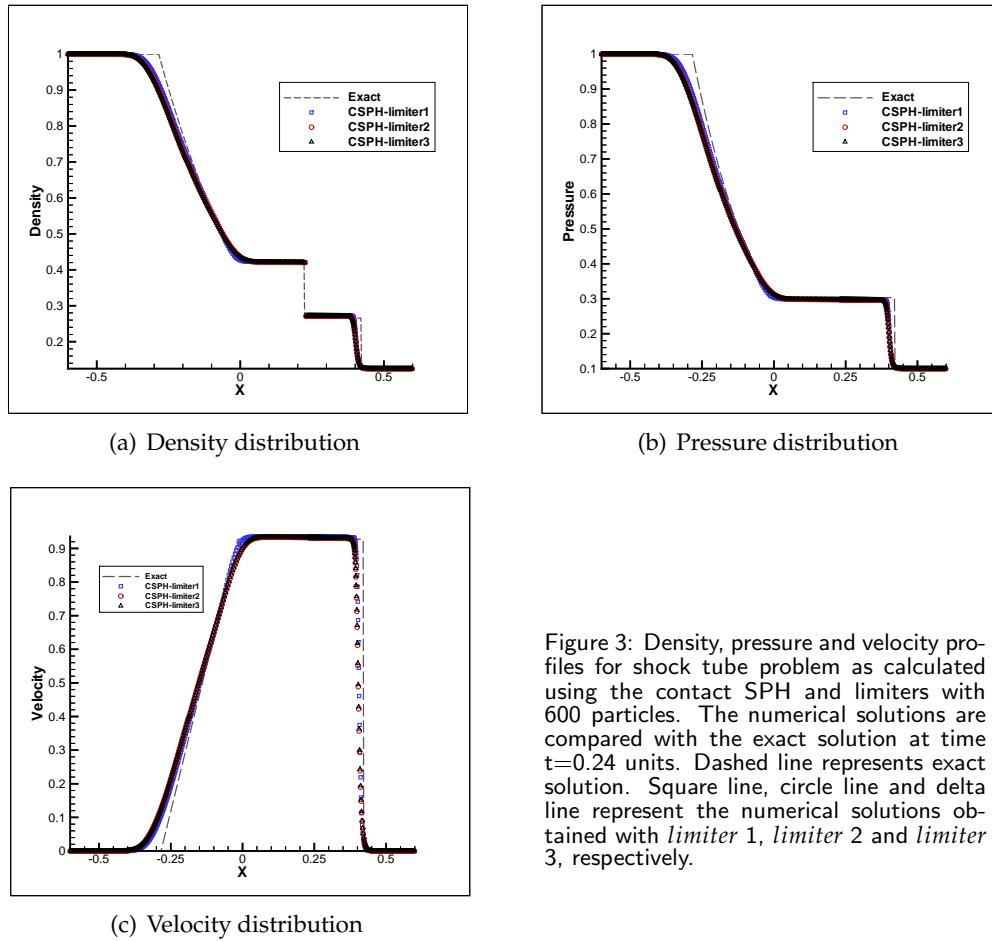


Figure 3: Density, pressure and velocity profiles for shock tube problem as calculated using the contact SPH and limiters with 600 particles. The numerical solutions are compared with the exact solution at time $t=0.24$ units. Dashed line represents exact solution. Square line, circle line and delta line represent the numerical solutions obtained with *limiter 1*, *limiter 2* and *limiter 3*, respectively.

using standard SPH without artificial viscosity a large amplitude oscillations are caused for the density, velocity and pressure in the whole star region of the flow. When contact solvers of the Riemann problem and limiter are introduced, the contact discontinuity is now very well solved. Across the contact discontinuity the velocity and pressure are continuous, while the density is discontinuous.

4.4 The blast wave

We now test the method on the blast wave problem used in [21], also see the literature [14]. The problem with shock Mach number approximate 200 involves extremely supersonic flows. The initial conditions are given by $\rho_L = 1$, $p_L = 1000$, $e_L = 2500$ for left-side state $x < 0$ and $\rho_R = 1$, $p_R = 0.01$, $e_R = 0.0254$ for right-side state $x > 0$, with $\gamma = 1.4$. For calculation, 1000 uniformly distributed particles are placed on each side of the initial discontinuity. The spatial range is $-1 \leq x \leq 1$. The initial spatial step is uniform $\Delta x = 0.001$

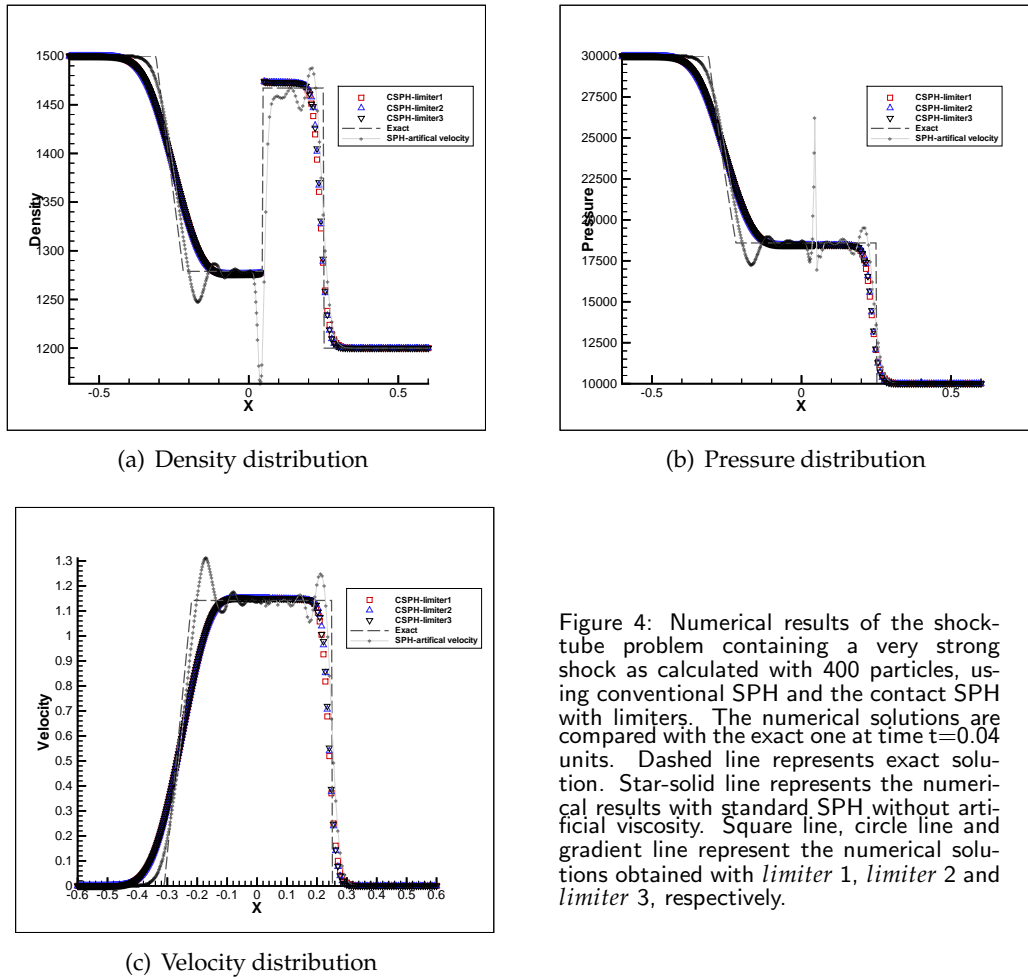


Figure 4: Numerical results of the shock-tube problem containing a very strong shock as calculated with 400 particles, using conventional SPH and the contact SPH with limiters. The numerical solutions are compared with the exact one at time $t=0.04$ units. Dashed line represents exact solution. Star-solid line represents the numerical results with standard SPH without artificial viscosity. Square line, circle line and gradient line represent the numerical solutions obtained with *limiter 1*, *limiter 2* and *limiter 3*, respectively.

and the initial smoothing length is set to $h_0 = 1.5\Delta x$. The calculation was carried out with a constant time step $\Delta t = 0.5 \times 10^{-6}$.

In contrast to above shock-tube test, the initial pressure of the gas on the left-hand side is 10^5 times that of the right-hand side. The blast wave problem is seen as a severe test which produces a sharp spike in the density variation just behind the shock. The conventional SPH does not work well for this test and gives an inaccurate description of the rarefaction wave and wrong post-shock values of the pressure and velocity, while the solution with the contact SPH and limiters matches the exact one.

The results for this test case are shown in Fig. 5 at $t=0.0075$. The position of the shock which locates at $x = 0.1764$ is very well compared with the exact solution denoted by dashed line. The density and pressure plots reproduce the analytical solutions with good accuracy except that there is a slight increment of the sharp density spike and a further reduction of the pressure plot in the star region of the flow.

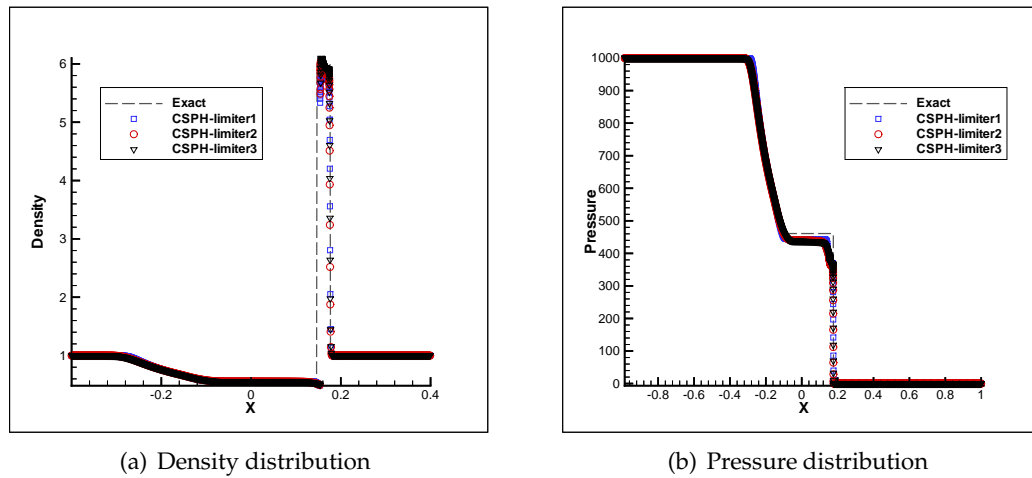


Figure 5: Numerical results for the blast wave problem as calculated using contact solvers of Riemann problem and three types of limiters with 1000 particles at time $t = 0.0075$ units. The numerical solutions are compared with the exact one. Dashed line represents exact solution. Square line, circle line and gradient line represent the numerical solutions obtained with *limiter 1*, *limiter 2* and *limiter 3*, respectively.

4.5 Collision of two strong shocks

We now consider the collision of two strong shocks which is the implosion of an ideal gas conceived in [21]. The initial conditions are given by $\rho_L = 1.0$, $v_L = 0$, $p_L = 0.01$ for left-side state $x < 0$ and $\rho_R = 1.0$, $v_R = 0$, $p_R = 100$. 1000 uniformly distributed particles are placed on spatial range $-1 \leq x \leq 1$. The calculation is carried out with a constant time step $\Delta t = 1 \times 10^{-5}$.

In particular, the problem is known to be a computationally intractable model producing a sharp spike in the density behind the shock. The conventional SPH fails to give the representation of wave fronts and correct post shock values of the density, pressure and velocity. Even, the computational process is probably terminated.

Fig. 6 compares the numerical solutions as obtained using contact SPH and three types of limiters. We also compare the simulated results with the exact solution denoted by dashed line at $t = 0.035$. Its solution consists of a left shock and a right rarefaction which are separated by middle contact discontinuity. We note that a sharp density spike forms when the two blast waves collide. The contact SPH with limiter may produce a more accurate solution except for the small wiggles in the density at the top of the contact discontinuity and shock wave, which in turn cause the oscillations in pressure and velocity plots. In addition, some weak disturbance is seen in front of rarefaction wave. The positions of contact discontinuity and shock wave match the exact solution.

From above examples it can be seen that the worst relative errors occur in the positions of the rarefaction heads and tails, the postshock values while the position of the contact discontinuity is well reproduced by the numerical solution. In contrast to grid-based formulations such as finite element method and finite difference method, the

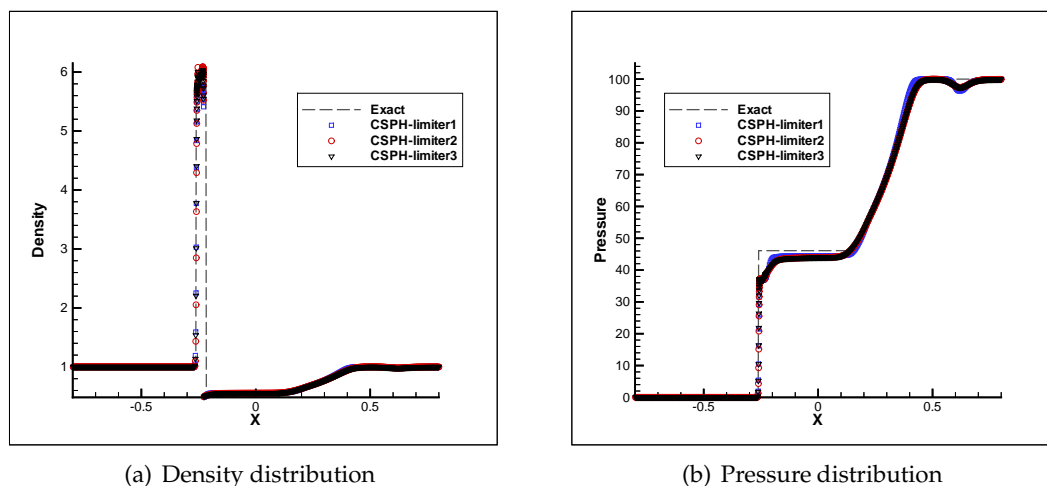


Figure 6: Numerical results for the collision of two strong shocks as calculated using three types of limiters as compared to the exact solution at time $t = 0.035$ units. Dashed line represents exact solution. Square line, circle line and gradient line represent the numerical solutions obtained with contact solution of Riemann problem and *limiter 1*, *limiter 2* and *limiter 3*, respectively.

shock-capturing scheme proposed here rely on the Riemann problem as a guide to improve SPH. In fact, it is not based on standard symmetrized representations of the SPH equations along with the usual kernel smoothing for the density so variational consistency of the scheme is not guaranteed.

5 Concluding remarks

In this paper, we have presented a class of contact SPH method suitable for inviscid compressible flow based on contact solvers of Riemann problem and different *limiters* which are first-order and second-order approximations. Combining high-order WENO interpolation with the limiter methods, the physical variables are reconstructed for interactional particles by Taylor series expansion. The obtained values are used as the initial values of the Riemann problem. The contact solvers and three types of *limiters* are introduced into discretization of control equations. We also briefly present some preliminary formulations on the possible extension of the contact SPH schemes of this paper to two-dimensional non-linear systems. The extension to nonlinear hyperbolic systems in 2D and 3D is the subject of ongoing research.

A number of one-dimensional numerical examples have been studied with comparisons to the results of conventional methods. The proposed method looks promising in capturing the sharper front of the shock and contact discontinuity. The obtained results suggest that the unexpected physical oscillations through the contact discontinuities can be prevented effectively and sharp interface can be captured accurately.

Acknowledgments

The authors would like to thank anonymous references for having provided a number of comments and suggestions that have greatly improved this paper. The work is partially supported by the Fundamental Research Funds of Central University(B103093) and Key Laboratory Foundation of Coastal Disasters.

References

- [1] Z. Wiezckowski, The material point method in large strain engineering problems, *Comput. Methods Appl. Mech. Engrg.*, 193 (2004), 4417-4438.
- [2] W. K. Liu, S. Jun, S. Li et al., Reproducing kernel particle methods for structural dynamics. *Int. Numer. Methods Eng.*, 38 (1995), 1655-1679.
- [3] J. J. Monaghan, On the problem of penetration in particle methods, *J. Comput. Phys.*, 82 (1989), 1-15.
- [4] C. Shu, H. Ding, H. Q. Chen, T. G. Wang, An upwind local RBF-DQ method for simulation of inviscid compressible flows, *Comput. Methods Appl. Mech. Eng.*, 194 (2005), 2001-2017.
- [5] C. S. Chen, S. Lee, C. S. Huang, The method of particular solutions using Chebyshev polynomial based function, *International Journal of Computational Methods*, 4 (2007), 15-32.
- [6] J. Campbell, R. Vignjevic, L. Libersky, A contact algorithm for smoothed particle hydrodynamics, *Comput. Methods Appl. Mech. Eng.*, 184 (2000), 49-65.
- [7] J. J. Monaghan, Simulating free surface flows with SPH, *J. Comput. Phys.*, 110 (1994), 399-406.
- [8] J. J. Monaghan, SPH and Riemann solvers, *J. Comput. Phys.*, 136 (1997), 298-307.
- [9] S. Inutsuka, Reformulation of smoothed particle hydrodynamics with Riemann solver, *J. Comput. Phys.*, 179 (2002), 238-267.
- [10] A. N. Parshikov, S. A. Medin, I. I. Loukashenko et al., Improvements in SPH method by means of interparticle contact algorithm and analysis of perforation tests at moderate projectile velocities, *International Journal of Impact Engineering*, 24 (2000), 779-796.
- [11] A. N. Parshikov, S. A. Medin, Smoothed particle hydrodynamics using interparticle contact algorithms, *J. Comput. Phys.*, 180 (2002), 358-382.
- [12] S. H. Cha, A. P. Whitworth, Implementation and tests of Godunov-type particle hydrodynamics, *Mon. Not. Royal Astron. Soc.*, 340 (2003), 73-90.
- [13] A. Ferrari, M. Dumbser, E. F. Toro, A. Armanini, A new stable and consistent version of the SPH method in Lagrangian coordinates, *SPHERIC-Smoothed Particle Hydrodynamics European Research Interest Community, 2nd International Workshop, Universidad Politécnic de Madrid, Madrid, 23-18 May, 2007*.
- [14] L. D. Sigalotti, H. López, A. Donoso, A shock-capturing SPH scheme based on adaptive kernel estimation, *J. Comput. Phys.*, 212 (2006), 124-149.
- [15] L. D. Sigalotti, H. López, L. Trujillo, An adaptive SPH method for strong shocks, *J. Comput. Phys.*, 228 (2009), 5888-5907.
- [16] J. P. Morris, P. J. Fox, Y. Zhu, Modeling low Reynolds number incompressible flows using SPH, *J. Comput. Phys.*, 136 (1997), 214-226.
- [17] J. J. Monaghan, Smoothed particle hydrodynamics, *Annu. Rev. Astron. Astrophys.*, 30 (1992), 543-574.
- [18] A. Colagrossi, M. Landrini, Numerical simulation of interfacial flows by smoothed particle hydrodynamics, *J. Comput. Phys.*, 191 (2003), 448-475.

- [19] R. A. Dalrymple, B. D. Rogers, Numerical modeling of water waves with the SPH method, *Coast. Eng.*, 53 (2006), 141-147.
- [20] C. W. Shu, Essentially non-oscillatory and weighted essentially non-oscillatory schemes for hyperbolic conservation laws, in: B. Cockburn, C. Johnson, C. W. Shu, E. Tadmor, A. Quarteroni (Eds.), *Advanced Numerical Approximation of Nonlinear Hyperbolic Equations*, Lecture Notes in Mathematics, Vol. 1697, Springer, New York, 1998, 325-432.
- [21] E. F. Toro, *Riemann Solvers and Numerical Methods for Fluid Dynamics: A Practical Introduction*, Third Edition, Springer, 2009.
- [22] G. R. Liu, M. B. Liu, *Smoothed Particle Hydrodynamics: A Meshfree Particle Method*, World Scientific, 2003.